Numerical Models in Geomechanics, Pietruszczak & Pande (eds) © 1997 Balkema, Rotterdam, ISBN 90 5410 886 X

Water movement effect on the strain localization during a biaxial compression

R.Charlier, J.P.Radu & J.D.Bamichon
MSM Department, Université de Liège, Belgium & ALERT Geomaterials

ABSTRACT : This paper is devoted to the numerical modelling of the strain localisation in a water saturated sample of soil, using a large strain finite element code. First an internal friction constitutive law is used. It includes a Lode angle dependency. Then the coupling with a pore fluid is considered, and the linkages between the seepage and the soil strain and stress evolution is taken in account through an effective stress postulate and an adaptation of the storage law. Coupled monolythical finite elements are developed. Unsaturated media are considered using the Bishop formulation and an adaptation of the seepage model. Finally the developed finite element code is applied to the modelling of the plane strain compression (including a strain localisation) of samples with different initial pore pressures and different drainage conditions. Drained case, undrained fully saturated and undrained partly saturated cases are considered.

1. INTRODUCTION

Strain localisation has been investigated in soils and in rocks for about two decades. Mainly drained behaviour has been studied in soils and rocks. However practically most of these materials are fully or partially saturated by water, oil, gas,... The question of the bifurcation to a localised strain mode in a biphasic soil remains quite open. Now it is particularly important for example in geotechnics (analysis of landslides, of foundation stability,...) or in tectonophysics (sedimentary basin evolution,...).

Only very few authors have proposed solution to the strain localisation problems for saturated soils. Desrues and Mokni (1992) have conducted experiments on localisation in undrained saturated sand. They performed a series of biaxial compression tests (in plane strain state) on Hostun sand in order to characterise the localisation appearance and the shear band mode. Vardoulakis (1995a, 1995b) and Han (1991) have conducted similar experiments on a clay. Loret and Prevost (1991) first have proposed some theoretical and numerical analysis of such problems. Schrefler (1996) has more recently proposed a finite element modelling of a multiphase localisation problem. But this analysis is limited to small strains problems and is based on dynamic and seepage coupled model.

The present paper is devoted to a finite element modelling of the strain localisation in a (partly) saturated soil sample during a biaxial compression. A Van Eekelen - Drücker Prager constitutive law is used. The hydromechanical coupling is based on the Terzaghi's postulate and on the storage law. Unsaturated behaviour is then derived as an extension of the previous equations. The developed finite element are monolythical : they are associating 2 displacements degrees of freedom and 1 water pressure one. The developed code is used to model some biaxial compressions in various states : drained, undrained saturated, undrained unsaturated and under different permeabilities.

2. SOIL CONSTITUTIVE LAWS

2.1 Stress invariants and stress space

I_σ, $II_{\hat\sigma}$, $III_{\hat\sigma}$ and β are defined as the first stress tensor invariant, the second deviatoric stress tensor invariant, the third deviatoric stress tensor invariant and the Lode angle, respectively

$$I_\sigma = \sigma_{ii} \tag{1}$$

$$II_{\hat\sigma} = \sqrt{\frac{1}{2}\hat\sigma_{ij}\hat\sigma_{ij}} \tag{2}$$

$$\hat\sigma_{ij} = \sigma_{ij} - \frac{I_\sigma}{3}\delta_{ij} \tag{3}$$

$$\beta = -\frac{1}{3}\sin^{-1}\left(\frac{3\sqrt{3}}{2}\frac{III_{\hat{\sigma}}}{II_{\hat{\sigma}}^{3}}\right), \text{ with } III_{\hat{\sigma}} = \frac{1}{3}\hat{\sigma}_{ij}\hat{\sigma}_{jk}\hat{\sigma}_{ki} \quad (4)$$

2.2 Mohr Coulomb criterion (MC)

The Mohr-Coulomb failure criterion is an intrinsic curve criterion. It expresses a linear relationship between the shear stress τ and the normal stress σ_N acting on a failure plane

$$\tau = c + \sigma_N \tan\phi \quad (5)$$

where c is the cohesion and ϕ the friction angle.

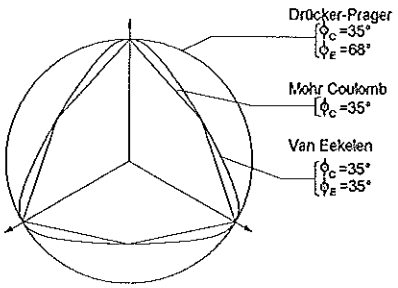

Figure 1. Limit surface for Mohr-Coulomb, Drücker-Prager and Van Eekelen criteria in the deviatoric plane.

This criterion predicts identical friction angles under triaxial compression paths (referred as ϕ_C) and triaxial extension paths (ϕ_E). Geometric representation of this criterion in the deviatoric plane gives an irregular hexagon (see figure 1). This model is not convenient to implement in the classical plasticity framework as the gradient of this yield surface is undefined on the hexagon corners. Therefore more continuously derivable yield surfaces are preferred.

2.3 Drücker Prager criterion (DP)

A simple approximation of the Mohr Coulomb surface has been proposed by Drücker and Prager, who defined the yield function f using a linear relationship between the first stress tensor invariant and the second deviatoric stress tensor invariant

$$f = II_{\hat{\sigma}} + \frac{2\sin\phi_C}{\sqrt{3}(3-\sin\phi_C)}\left(I_\sigma - \frac{3c}{\tan\phi_C}\right) = 0 \quad (6)$$

In the principal stress space, the plasticity surface becomes a cone which is much easier to use in numerical algorithms. The trace of this plasticity surface on the deviatoric plane is then a circle (see figure 1). Although this simple criterion is widely used in geomechanics to represent frictional behaviour, it does not depend on the third stress invariant and thus on the Lode angle β. This is a main drawback of this model.

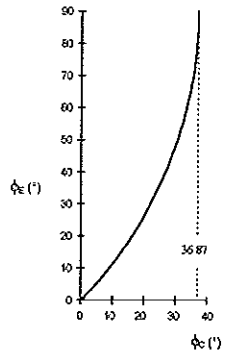

Figure 2. ϕ_E versus ϕ_C for Drücker-Prager criterion.

The radius is constant in the Drücker Prager model, this yields

$$\sin\phi_E = \frac{3\sin\phi_C}{3-\sin\phi_C} \Big/ 1 - \left(\frac{\sin\phi_C}{3-\sin\phi_C}\right) \quad (7)$$

A plot of ϕ_C versus ϕ_E computed from equation (7) is given on figure 2 and shows that ϕ_E does not increase linearly with ϕ_C. There is a limit value of ϕ_E=90° for $\phi_C \approx 36.87° = \phi_C^{lim}$.

If non-associated plasticity is considered, a plastic potential g can be defined in a similar fashion than the yield surface f replacing ϕ by ψ in equations (6).

2.4 Van Eekelen criterion (VE)

A more sophisticated model can be built from the Drücker-Prager cone by introduction of a dependence on the Lode angle β in order to match more closely the Mohr Coulomb criterion. It consists in smoothing the Mohr Coulomb plasticity surface. The formulation proposed by Van Eekelen (1980) is adopted

$$f = II_{\hat{\sigma}} + m\left(I_\sigma - \frac{3c}{\tan\phi_C}\right) = 0 \quad (8)$$

with the coefficient m defined by

$$m = a(1 + b\sin 3\beta)^n \qquad (9)$$

The only difference between DP and VE criteria comes from the point that the coefficient m is constant for DP whereas it is a function of the Lode angle for VE. Coefficients a and b allow an independent choice for ϕ_C and ϕ_E . The exponent n actually controls the convexity of the yield surface. Following the conclusion of Van Eekelen (1980), the default value n=-0.229 has been chosen. The trace of this plasticity surface in the deviatoric plane is displayed on figure 2. If non-associated plasticity is considered, a flow potential g can also be defined in a similar fashion than the plastic potential f.

2.5 Comparison between Mohr Coulomb, Drücker Prager and Van Eekelen criteria

At very low friction angles, the three criteria are pretty much similar. The difference between the DP criterion on the one hand and the MC or VE criteria on the other hand increases as friction angle gets larger. This is directly linked to the relation between ϕ_C and ϕ_B : from equation (7) it is found that for DP ϕ_B=26° for ϕ_C=20°. However as friction angle ϕ_C gets closer to the limit value 36.89°, the corresponding angle ϕ_E approaches 90°. Therefore if low friction angles are considered (let say below 20°), the three criteria will give approximately the same results. However, above this value of 20°, some significant differences can be expected between the DP criterion on the one hand and the MC or VE criteria on the other hand.

3. LARGE STRAINS IN SOLID MECHANICS

Strain localisation is generally associated to large strains and large rotations. The strain amount observed inside the hereafter modelled shear bands can as high as 50% to 100%. In the following the mechanical equilibrium is formulated in the current configuration using the Cauchy stresses. The Jaumann correction is used in order to give an objective stress rate.

When a small strain formulation is assumed, the strain decomposition between its elastic and plastic parts is assumed. In a large strain formulation one often postulates an unloaded configuration, which is leading to a multiplicative decomposition of the elastic and plastic Jacobian matrix :

$$\underline{F} = \underline{F}^p \underline{F}^e \qquad (10)$$

We assume here that the elastic part of the deformation is small compared to the unity. This yields an approximately additive decomposition of the strain rate :

$$\underline{D} = \underline{D}^E + \underline{D}^P \qquad (11)$$

4. FLOW IN POROUS MEDIA

In a saturated porous medium, flow is assumed to follow the Darcy's law :

$$\underline{v} = -K\,\underline{\nabla}\left(\frac{p}{\gamma} + z\right) \qquad (12)$$

where K is the permeability, p the pore pressure, z the level, γ the fluid specific weight and $\underline{v}$ the Darcy's velocity. If partly saturation is to be considered, the Darcy's law (12) can be used assuming that the permeability K is varying with the saturation degree :

$$K = K(S_r) \qquad (13)$$

We will suppose hereafter that this law is a linear one

$$K = K_0 S_r \qquad (14)$$

The storage law is giving the evolution of the amount of fluid mass per unit of soil volume. When the fluid saturation degree S_r is varying, two storage terms are to be taken in account :

$$\dot{S} = n\frac{\dot{p}}{\chi_w} + n\dot{S}_r \qquad (15)$$

When two fluids are partly saturating the pores, two sets of equations (12-15) should be written. However if one fluid is a gas, its behaviour can be neglected, considering that its pressure remains quite constant, or equivalently that it is highly compressible.

On the other hand it is necessary to formulate a retention curve associating the saturation degree to the suction s (which is the difference between the non-wetting and the wetting fluid pressures). We here are using the following relation :

$$S_r = \frac{1}{\pi} arctg\frac{s-\beta}{\alpha} + \frac{1}{2} \qquad (16)$$

$$s = p_{gas} - p_{liquid}$$

When considering a water saturated and dilatant soil under shear loading (e.g. in the hereafter considered biaxial compression) the material tends to dilate but the pore fluid (which is quite incompressible) does not allow that. The fluid pressure therefore decreases from its initial value (generally a back-pressure imposed to ensure the good saturation by dissolving air in water). When the water pressure tends to the atmospheric pressure, the dissolved air appears as bubbles. The fluid is now biphasic, what means that the soil is partly saturated

in air and water. If the initial air content is low enough, a similar desaturation will appear when cavitation will occur. In that case the gas is composed of water vapour bubbles. Whatever the way the soil becomes partly saturated, the fluid compressibility increases quickly at that time. This phenomenon will be simply modelled by using a retention curve postulating a desaturation around the atmospheric pressure.

5. HYDROMECHANICAL COUPLING

Stresses are affected by the seepage. This is modelled for saturated media by the Terzaghi's postulate. It is here written in an incremental form:

$$\dot{\underline{\sigma}} = \dot{\underline{\sigma}}' - \dot{p}\underline{I} \qquad (17)$$

If the soil is partly saturated by two fluids, this postulate is not more valid. Bishop has proposed a modified form :

$$\dot{\underline{\sigma}} = \dot{\underline{\sigma}}' - \chi(S_r)\dot{p}\underline{I} \qquad (18)$$

where $\chi(S_r)$ is a new function to be defined from experimental results. This relation can be analysed as a mixture law (Schrefler, 1990). It becomes then :

$$\dot{\underline{\sigma}} = \dot{\underline{\sigma}}' - S_r\dot{p}_{liquid}\underline{I} - (1-S_r)\dot{p}_{gas}\underline{I} \qquad (19)$$

On the other hand, the fluid flow is affected by the soil mechanics through the storage law in which the pores volume is modified according to the volumetric strain rate :

$$\dot{S} = n\frac{\dot{p}}{\chi_w} + n\dot{S}_r + \dot{\varepsilon}_{ii} \qquad (20)$$

In this equation, it is supposed that the soil grains (or the soil skeleton) volume does not change with respect to the mean effective stress variation.

The soil mechanics is involving large strains. This does not affect the fluid flow in the sense that the balance equation is formulated at one instant per time step (generally at the step end). Moreover the storage and Darcy's flow laws are not depending on the history. Therefore no objective correction is needed. On the other hand, the additive strain decomposition (11) is here assumed to remain valid (Bourgeois et al (1995)).

The hydromechanical coupling is implemented in the finite element code LAGAMINE trough a monolythical scheme, which has proved to be efficient for the considered problems.

6. APPLICATION

We consider in the following the biaxial compression which is a classical test for the study of the strain localisation in soils (Mokni and Desrues (1992), Vardoulakis (1991, 1995 a & b). A parallelepiped sample of soil is under plane strain conditions. Two sample sizes are considered : 175 x 350 mm^2 (rectangular) and 164 x 173 mm^2 (square). The initial stress state is isotropic. A pressure is applied to the lateral boundaries. It remains constant during the axial loading. The lower base lies on a frictionless platen ; the upper one is compressed by a second frictionless platen.

6.1 Rectangular sample

The initial stress state is σ'_0 = 100 kPa. The sample is discretised by 10 x 20 8-nodes finite elements. The soil is modelled by an elastic - perfectly plastic Drücker-Prager model whose parameters are indicated in table 1. The seepage parameters are given in the same table. The compression velocity (upper plateau) is $\dot{H} = 1{,}8\ 10^{-3}\ mm/s$. Some different cases have been modelled. Most results are not illustrated here, due to the lack of space.

table 1 : Rectangular sample - mechanical and seepage parameters.

parameter	symbol	value
Young modulus	E	2.6 GPa
Poisson's ratio	ν	0.3
compression friction angle	ϕ_c	25°
dilatancy angle	ψ	10°
water compressibility	χ_w	3. GPa
porosity	n	0.45

Case 1 : It corresponds to a drained sample. A shear band clearly appears, as generally under such kind of condition. Small imperfections have been introduced in order to help this bifurcation. However it should be noted that numerical imperfection are sufficient to induce the strain localisation.

Case 2 : The sample is fully saturated by water and the initial back-pressure is high enough to avoid any cavitation or other de-saturation. The permeability is low : $K=10^{-20}$ ms^{-1}. The mesh remains rectangular and the stress and pore pressure state is homogeneous during the whole compression process. The global volume remains constant. The volumetric strains are zero. The pore pressure variation is Δp = 500 kPa at the end of the simulation.

Case 3 : The permeability is much more larger than in the preceding example: $K=10^{-7}$ ms^{-1}. Two shear bands now appear. The global volume remains

always constant. However the volumetric strains are not homogeneous (figure 3) and varies from about 4% dilatation inside the band to about 1.5% contraction outside it. This is allowing the necessary dilation inside the shear bands, and explains why they are appearing as in the drained case.

According to these variations of the void ratio the water storage and the pore pressure are also varying. It results in pressure gradients and in water flows. These Darcy's velocities are showing that the two shear bands are not always active together.

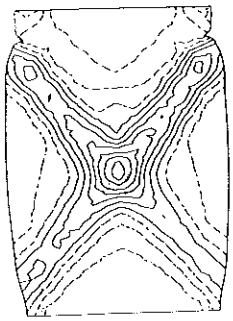

Figure 3 : Case 3 : volumetric strains in the deformed mesh after 15 % of axial strain.

6.2 Square sample

The initial stress state is $\sigma'_0 = 100$ kPa. The sample is discretised by 30 x 30 8-nodes finite elements. The soil is modelled by an elastic - perfectly plastic Van Eekelen model whose parameters are given in table 2. The seepage parameters are indicated in the same table. Globally undrained states are considered. Therefore the total pore fluid mass remains constant. An initial back-pressure $p_0 = 30$ kPa is applied. The rate of displacement of the upper boundary is 10^{-3} $\%.s^{-1}$ (of the initial height).

table 2 : Square sample: mechanical and seepage parameters.

parameter	symbol	value
Young modulus	E	35 MPa
Poisson's ratio	ν	0.4
compression friction angle	ϕ_c	41°
extension friction angle	ϕ_e	41°
dilatancy angle	ψ	10°
permeability	K	10^{-16}m/s
water compressibility	χ_w	3. GPa
porosity	n	0.3

No strain localisation is apparent from the deformed mesh. However the water pore pressure map shows clearly a localisation band where the pore pressure has highly decreased (from 130 kPa initially to -120 kPa after 9% of axial deformation -figure 4). The water pore pressure has decreased because of the band dilatancy. A little later (10% compression) the localisation scheme has changed (figure 5) and two localised band have appeared. The water pressure is a little lower (-160 kPa). These negative pore pressures are associated with a partial saturation (cf. retention curve). At the band centre the saturation degree has decreased to 95%.

The sample shearing concentrates in the band and it is associated with a local volume increase. Water accommodates this by decreasing its pressure. Due to the resulting pressure gradient water flow from outside the band to inside it (figure 6).

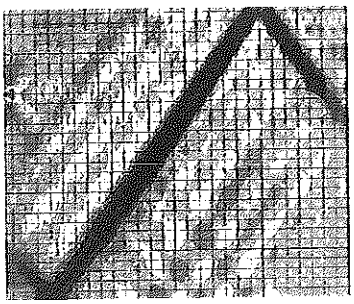

Figure 4. Contours of water pressure after 9 % compression.

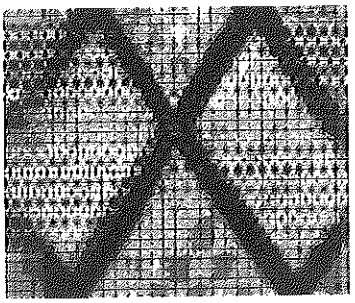

Figure 5. Contours of water pressure after 10 % compression.

7. CONCLUSIONS

A hydromechanical large strains finite element code has been developed for soils and rocks modelling. It has been applied to the modelling of biaxial compressions on various soil samples.

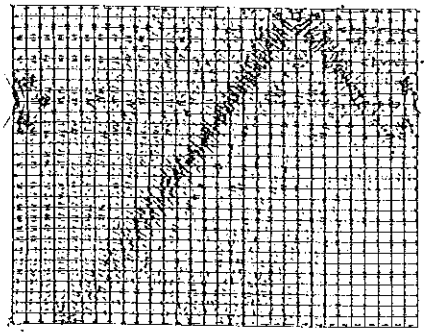

Figure 6. Water flow - Darcy's velocities after 10% compression.

Pure mechanical analysis (on drained samples) shows clearly a strain localisation. The modelling is possible up to very large strains.

In a saturated soil sample, if the permeability is small enough compared to the loading velocity, water has not enough time to move during any strain localisation process. Then the unsaturated state is a global and a local one. No strain localisation can appear.

In a dilatant sample the pore pressure is continuously decreasing during the stress deviator increase (uniaxial compression phase). When that pressure becomes small enough, gas bubbles are appearing due to cavitation in pure water or to the end of air dissolution in other cases. Then the pore fluid becomes a biphasic one with a high compressibility, and a drained like localisation is possible.

If the permeability is larger, then water moves and allows a strain localisation in a dilatant medium. The undrained condition is a global one. This means that the total volume remains constant due to the low fluid compressibility. However at a local level, dilatancy as well as contractancy are appearing. The volumetric strain integral over the whole sample volume is quite null (with respect to the fluid compressibility).

ACKNOWLEDGEMENTS

The authors are grateful to the *Groupement de Recherche en géomécanique des Roches Profondes,* to the EC through the financial support to the network *ALERT Geomaterials,* and to the FNRS.

REFERENCES

E. BOURGEOIS, P. de BUHAN et L. DORMIEUX. Formulation d'une loi élastoplastique pour un milieu poreux saturé en transformation finie. C.R. Acad.Sci, Paris, t.321, Série IIb, pp. 175-182, 1995.

M. MOKNI Relations entre déformations en masse et déformations localiseés dans les matériaux granulaires. Thesis UJF-INPG, Grenoble, 1992.

B. LORET, J.H. PREVOST Dynamic strain localization in fluid-saturated porous media. Jl. of Eng. Mech. Vol. 117, N° 4, pp. 907-922, 1991.

B.A. SCHREFLER, L. SIMONI, X.K. LI, O.C. ZIENKIEWICZ. Mechanics of partially saturated porous media. Numerical Methods and Constitutive Modelling in Geomechanics. C.S. Desai and G. Gioda, ed., CISM Courses and Lectures, N° 311, Springer Verlag, 169-209, 1990.

B.A. SCHREFLER, L. SANAVIA and C.E. MAJORANA. A multiphase medium model for localisation and postlocalisation simulation in geomaterials. Mechanics of Cohesive Frictional Materials, Vol. 1, 95-114 (1996).

C. HAN and I.G. VARDOULAKIS. Plane strain compression experiments on water-saturated fine-grained sand. Géotechnique 41, N° 1, pp. 49-78, 1991.

H.A.M. van EEKELEN. Isotropic yield surfaces in three dimensions for use in soil mechanics. Int. Jl. for Numerical and Analytical Methods in Geomech., Vol.4, 89-101, 1980.

I.G. VARDOULAKIS. Deformation of water-saturated sand: I. Uniform undrained deformation and shear banding. Géotechnique, 46, n° 3, 441-456, 1995.

I.G. VARDOULAKIS. Deformation of water-saturated sand: II. The effect of pore water flow and shear banding. Géotechnique, 46, n° 3, 457-472, 1995.